Magnetic Resonance in Medicine 43:503–509 (2000)

Phase-Contrast With Interleaved Undersampled Projections

A.V. Barger,[1*] D.C. Peters,[1] W.F. Block,[2] K.K. Vigen,[2] F.R. Korosec,[2,3] T.M. Grist,[3] and C.A. Mistretta[2,3]

MR phase-contrast techniques provide velocity-sensitive angiograms and quantitative flow measurements but require long scan times. Recently it has been shown that undersampled projection reconstruction can acquire higher resolution per unit time than Fourier techniques with acceptable artifacts when used in contrast-enhanced MR angiography. Undersampled projection reconstruction has similar potential for phase-contrast acquisitions. Flow sensitization gradients are used with projection trajectories to acquire velocity-dependent phase information. An acquisition scheme that acquires three flow encoding directions on three sets of angular-interleaved projections is introduced. Depending on the resolution, acquisition times for 3D datasets can decrease by factors of two to four. Magn Reson Med 43:503–509, 2000. © 2000 Wiley-Liss, Inc.

Key words: velocity imaging; fast magnetic resonance imaging; phase-contrast; projection reconstruction

Phase-contrast methods differentiate moving spins by using a gradient waveform with a nonzero first moment to impart a phase shift proportional to the velocity of the spin (1,2). In one implementation a symmetric bipolar gradient is applied on a given Cartesian axis prior to spatial encoding. A stationary proton will accumulate zero net phase from the bipolar gradient, whereas a proton moving along the chosen axis will acquire a net phase offset that can be converted into a velocity value. A second acquisition with an inverted bipolar gradient is used to correct for phase offsets not related to flow, such as those caused by magnetic field nonuniformity, eddy currents, and RF pulse effects. Velocity images can then be generated using either complex-difference (3) or phase-difference (4) methods.

Although phase-contrast techniques can both produce qualitative angiographic images and provide a quantitative measure of flow, 3D phase-contrast imaging is not widely used clinically. 3D phase-contrast imaging has at least two major drawbacks. First, the acquisition time of a 3D high-resolution spin-warp phase-contrast image with flow encoding on all three axes is prohibitively long for clinical applications. Second, pulsatile flow causes ghosting artifacts with ungated spin-warp phase-contrast imaging. The addition of gating to the sequence removes the pulsatility artifacts but increases the scan time to clinically unfeasible lengths for even a low-resolution acquisition (5). The most commonly used noncontrast enhanced technique for imaging moving spins is time-of-flight angiography, which relies on differences in magnitude of saturated tissue and unsaturated blood for contrast. Time-of-flight techniques have been used to calculate quantitative flow information (6,7) but the analysis depends on a specific model of the effects of blood flow wash-in and has not gained widespread use.

There have been many proposed alternatives to conventional phase-contrast imaging based on echo-planar, spiral, and other techniques. 2D EPI phase-contrast imaging has short acquisition times, but has high phase sensitivity to motion in the phase blip direction (8). Spiral 2D phase-contrast imaging greatly shortens scan times and also reduces the appearance of pulsatility artifacts in the image but is very sensitive to off-resonance effects and requires the acquisition of a magnetic field map before the image acquisition (9).

We developed a phase-contrast sequence termed PIPR (Phase-contrast with Interleaved Projections) to address some of the problems of phase-contrast imaging. PIPR acquires phase-contrast data using an undersampled projection technique. Undersampled projection reconstruction has recently been shown to provide higher resolution per unit time than spin-warp encoding with a minimum of artifacts in contrast-enhanced MR angiography (10). We have taken advantage of undersampling the projections to either reduce the total scan time or to increase the spatial resolution for a given scan time. We found that for phase-contrast acquisitions the degree of undersampling can be even larger than for contrast-enhanced applications because background tissue is subtracted and does not generate artifacts. In addition to undersampling the projections, we use an interleaving strategy to further reduce the appearance of artifacts in composite images. As the projection angle is incremented, velocity encoding is cyclically performed in the x, y, and z directions. This acquisition strategy results in three sets of interleaved projections, one set for each velocity component, and minimizes the appearance of streaks by reducing the coherent addition of the artifacts.

MATERIALS AND METHODS

Pulse Sequence

The pulse sequence for a 3D phase-contrast projection reconstruction sequence is shown in Fig. 1. The technique is an extension of the projection reconstruction gradient-echo sequence previously described by our group (10). The bipolar flow encoding gradient G_{BP}, which can be positive (as depicted) or negative (inverted), follows the RF excita-

[1]Department of Physics, University of Wisconsin, Madison, Wisconsin.
[2]Department of Medical Physics, University of Wisconsin, Madison, Wisconsin.
[3]Department of Radiology, University of Wisconsin Medical School, Madison, Wisconsin.

Grant sponsor: NSF; Grant number: BES 7908319.

*Correspondence to: A.V. Barger, Department of Radiology (E3/311), Clinical Sciences Center, 600 Highland Avenue, Madison, WI 53792-3252. E-mail: abarger@mr.radiology.wisc.edu

Received 2 August 1999; revised 12 January 2000; accepted 13 January 2000.

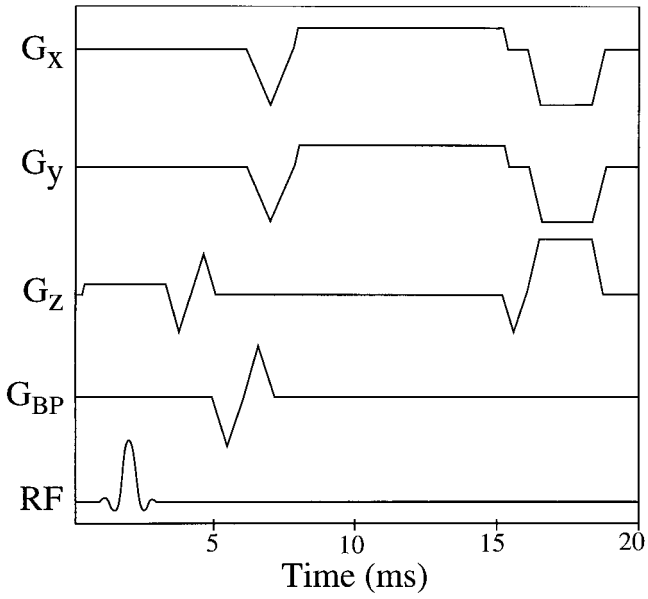

FIG. 1. Projection reconstruction phase-contrast pulse sequence. RF excitation is followed by either a positive or negative bipolar flow-encoding pulse G_{BP} that can be placed on any of the three axes. The readout gradients G_x and G_y are shown at their maximum strength, but the amplitudes are varied to trace out projections at different angles. Readout gradients are followed by rewinding gradients and a spoiler gradient is applied in the slice select direction.

tion pulse and can be placed on any axis. The first moment of the bipolar pulse, and thus the amplitude, is set by the maximum velocity to be encoded (VENC). The bipolar pulse is added to the G_x, G_y, or G_z waveform with combined gradient lobes to minimize the echo time and thereby reduce flow dephasing (11). The operator can choose to encode on the *x*, *y*, or *z*-axis individually or on all axes with PIPR. If velocity is to be encoded along all three axes, the bipolar pulse is alternately placed on the *x*, *y*, and *z*-axes on a projection-by-projection basis with increasing angles, as shown in Fig. 2a. Because every velocity encoding is at a different projection angle, reducing the number of velocity encodings from six to four, as performed in spin-warp acquisitions (12), is not possible. Instead, two projections are acquired at every angle using "two-sided" flow encoding with both a positive and a negative bipolar pulse.

Projections are acquired with a rotating in-plane readout gradient. Figure 2 shows two different projection angle sampling schemes, either acquiring projections over 180° (Fig. 2a) or over 360° (Fig. 2b). Since the sequence uses a 75% fractional echo, the two angular distributions are not equivalent. The 180° acquisition has an asymmetric *k*-space sampling, whereas the 360° acquisition has a more uniform but sparser sampling of the outer regions of *k*-space. In the 360° acquisition the projections are chosen at offset angles so the same angle is not acquired twice. Conventional Fourier phase encoding is performed along the *z* direction.

Since steady state is not reached at the end of the readout, rewinders are used on the *x* and *y* axes to return to the center of *k*-space. A *z*-gradient spoiler is applied during the time that the rewinding gradients are played. The operator can also choose to employ flow compensation during the sequence.

The pulse sequence was implemented on a 1.5 T Signa system (GE Medical Systems, Milwaukee, WI). The repetition-time (TR) of the sequence depended on the specific scan parameters but was typically 21 ms. The echo-time (TE) of the sequence was typically 7 ms with a 75% fractional echo.

Reconstruction

The raw data is saved on the scanner for off-line analysis. All image reconstruction is implemented on a Silicon

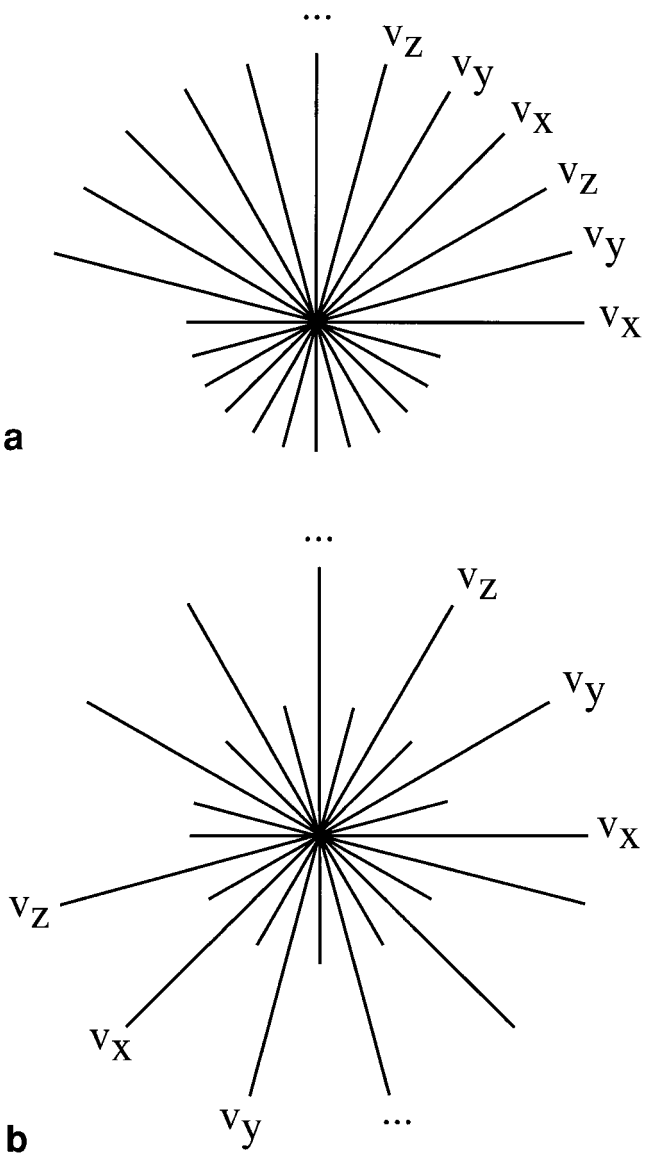

FIG. 2. Diagram of two possible projection angular sampling schemes. The 180° acquisition (**a**) achieves the closest sampling density in outer regions of *k*-space but has asymmetric coverage of *k*-space due to the fractional echo. The 360° acquisition (**b**) has larger angular spacing of projections in outer regions of *k*-space but also has a more uniform coverage of all regions of *k*-space.

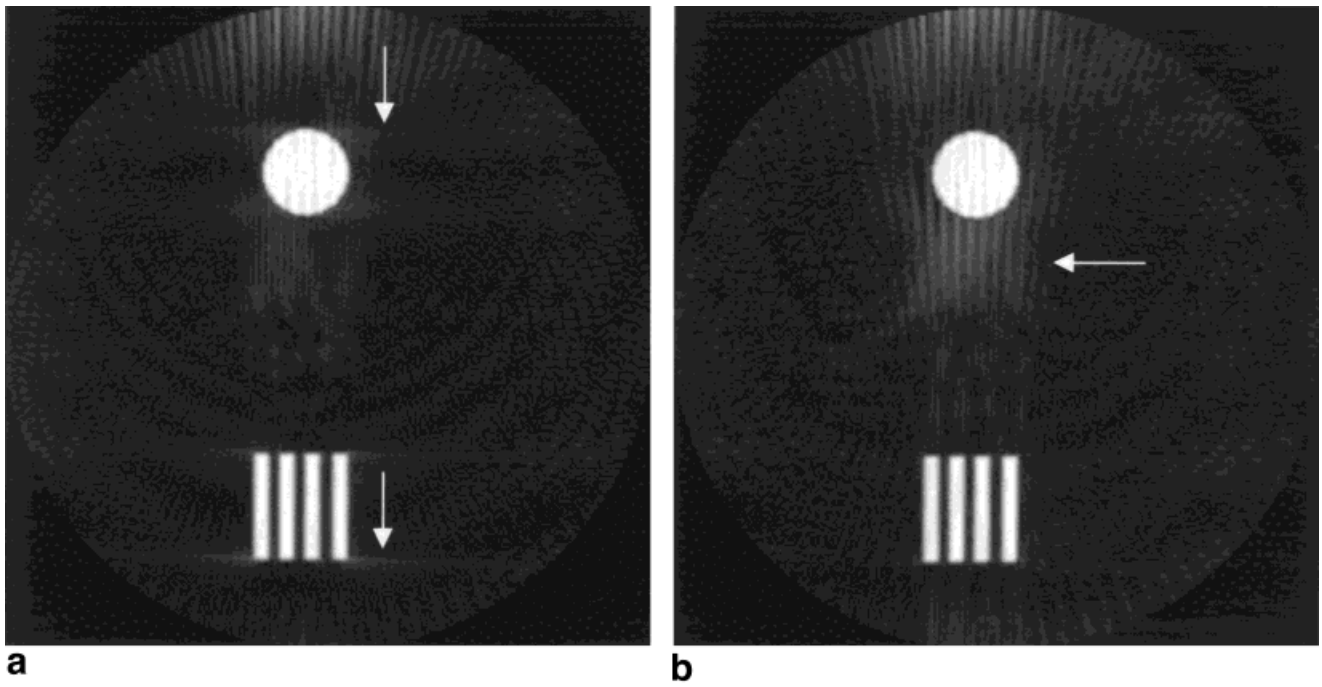

FIG. 3. Simulation of the effects of a 180° (**a**) and 360° (**b**) fractional echo acquisition combined with an off-center *k*-space. The smearing artifacts pointed to by the arrows in **a** are noticeable with the 180° acquisition, while streaking artifacts pointed to by the arrow in **b** are worse with the 360° acquisition.

Graphics Onyx 2 workstation (SGI, Mountain View, CA). The raw data is first Fourier-transformed in the *z*-direction. For PIPR acquisitions the projections are separated into three sets (corresponding to the flow encoding directions) and each set is reconstructed individually.

The real and imaginary channels of the filtered projections are backprojected separately (a process henceforth referred to as complex backprojection). Projections are filtered using a Ram-Lak filter (13). Two complex images are generated corresponding to the positive and negative bipolar acquisitions. Complex difference and phase difference subtraction is applied at each pixel between the two images to generate complex difference and phase difference images. Although we currently use complex backprojection to reconstruct the image, regridding techniques could also be used.

To form the final complex difference image for PIPR, a composite image including information from all three velocity-encoding directions is calculated from the magnitude of the 3D velocity-image vector. Individual phase difference images are used to calculate quantitative flow values by a standard phase-contrast procedure. The phase in the phase difference image is converted into a velocity value using the prescribed VENC. A region of interest (ROI) is drawn on the boundary of the vessel and the area of each pixel is calculated from the scan parameters. The flow is calculated by summing the product of the velocity in each pixel and the pixel area.

Simulations and Phantom Experiments

Computer simulations were calculated using Alice (Hayden Image Processing Group, Boulder, CO). 128 projections with a readout length of 256 were computed from a purely real object. These projections were Fourier-transformed and truncated to simulate a fractional echo. To simulate the effect of eddy currents the projections were shifted by 0.125 pixel in the *k*-space domain. The data was then Fourier-transformed back into image space and complex backprojected to produce the final reconstructed image.

Phantom studies were performed with a computer-controlled flow pump (Quest Image, London, Ontario, Canada). The pump allowed the volume flow rate to be set with a precision of 0.1 ml/sec and also allowed for variable flow patterns. The fluid used in the pump and tubing was a mixture of distilled water and Syn-Cut H.D. machining oil (Acra Tech, Boucherville, Quebec, Canada) which was chosen for its ability to mimic the MR properties of blood. Only flow in the *z*-direction was encoded for these experiments. The FOV was 12 × 12 cm, slice thickness 4 mm, and the VENC 50 cm/sec. Spin-warp phase-contrast images were acquired at 256 × 256 using an ungated 2D phase-contrast sequence with one NEX. Projection reconstruction images were acquired using an ungated 2D sequence with a readout resolution of 256 and with 64 total projections (128 excitations). In one experiment the flow pattern was set to simulate that of the carotid artery and was imaged with both projection and spin-warp techniques. In the second experiment a flow quantification study was performed for projection techniques using a simple tube phantom with constant flow rates ranging between 1.5 ml/sec and 6.0 ml/sec.

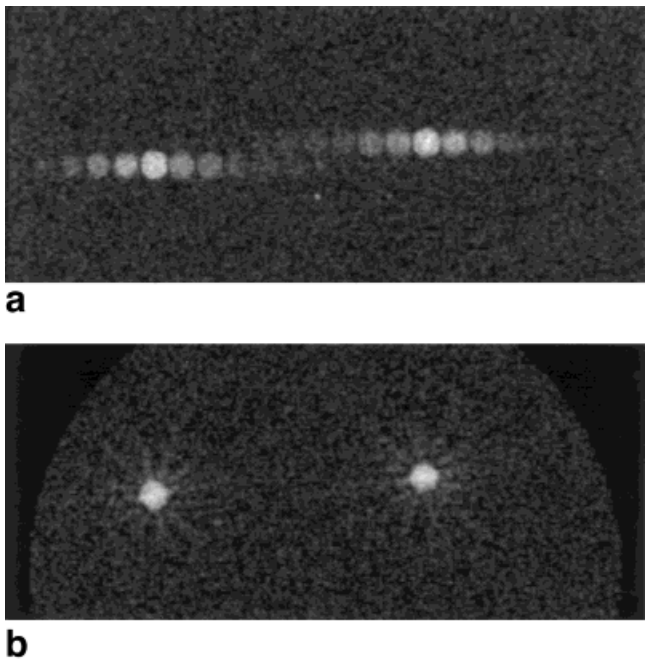

FIG. 4. Comparison of pulsatility artifacts seen in spin-warp phase-contrast imaging (**a**) and in projection reconstruction imaging using 64 projections (**b**). The phantom was a tube in a loop with simulated carotid flow. The pulsatility artifacts, which appear as ghosts in **a**, manifest as slight streaks radiating from the tube in **b.**

Volunteers

Two volunteers were scanned with both conventional phase-contrast and PIPR sequences after obtaining informed consent. We imaged the circle of Willis, since its variety of flow directions, flow rates, and vessel sizes provide a good overall test for the sequence. A quadrature head coil was used to image a region covering the circle of Willis with the most inferior slice located at the tip of the basilar artery. A 30° flip angle was used for the RF pulse.

In one volunteer both PIPR and spin-warp acquisitions were prescribed using 32 slices with 2 mm slice thickness. PIPR images were acquired with 512 and 256 readout points and 192 total projections in both cases (64 projections for each flow direction). The 256 PIPR image had a FOV of 24 × 24 cm, whereas the 512 PIPR image had a FOV of 30 × 30 cm, so effectively there were 410 readout points over the 24 cm FOV. Cartesian trajectory phase-contrast images were acquired with 256 and 128 phase-encoding values using 256 readout points in both cases. Higher resolutions were not feasible due to long scan times (>20 min).

In the second volunteer only a 256 readout resolution for both the PIPR and the spin-warp acquisition was used. The PIPR acquisition was prescribed with 64 total slices with 0.9 mm slice thickness. The total number of projections used was 180, resulting in a scan time of 8 min 4 sec. The corresponding Fourier scan was prescribed with 32 total slices and 2 mm slice thickness. The number of phase encoding values was 192 and the scan required 8 min 36 sec.

RESULTS

Simulations

Figure 3 demonstrates the effects of 180° vs. 360° angular sampling with simulated off-resonance conditions. The 180° (Fig. 2a) angular sampling results in a horizontal smearing of the objects (arrows in Fig. 3a). When the angular sampling of projections spans 360° (Fig. 2b), there is a more even coverage of *k*-space and the smearing artifact is reduced. However, because the outer regions of *k*-space are now sampled farther apart, streak artifacts are more pronounced in the final image (arrow in Fig. 3b). The two techniques are best suited for different applications due to differences in the generated artifacts. Quantitative flow measurements require well-defined object borders for calculating the area of the vessel. In this case, projections spanning 360° define the borders of the object without any smearing. For qualitative images, we have found that the smearing artifact resulting from a 180° acquisition is less distracting than the increased streak artifacts from a 360° acquisition.

Phantom Experiments

Images of a simple tube phantom with a pulsatile flow pattern simulating that of the carotid artery are shown in Fig. 4. In the standard phase-contrast image (Fig. 4a) the flow pulsatility results in multiple bright ghost images of the tube along the phase-encoding direction. In the projection reconstruction phase-contrast image the flow pulsatility results in slight streak artifacts originating from the object (Fig. 4b).

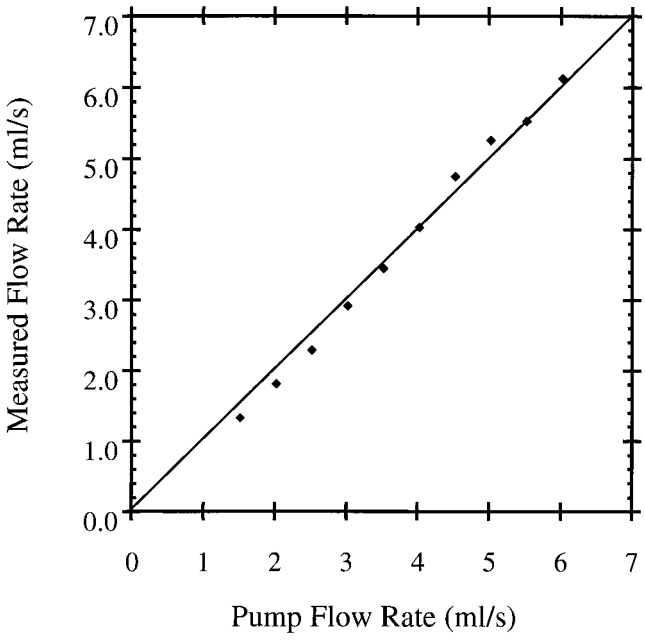

FIG. 5. Plot of measured flow values using a projection reconstruction phase-contrast acquisition with 64 projections (data points) vs. the expected relationship (line). A linear fit to the data points results in a slope of 1.093, whereas the expected relationship line has a slope of 1.0.

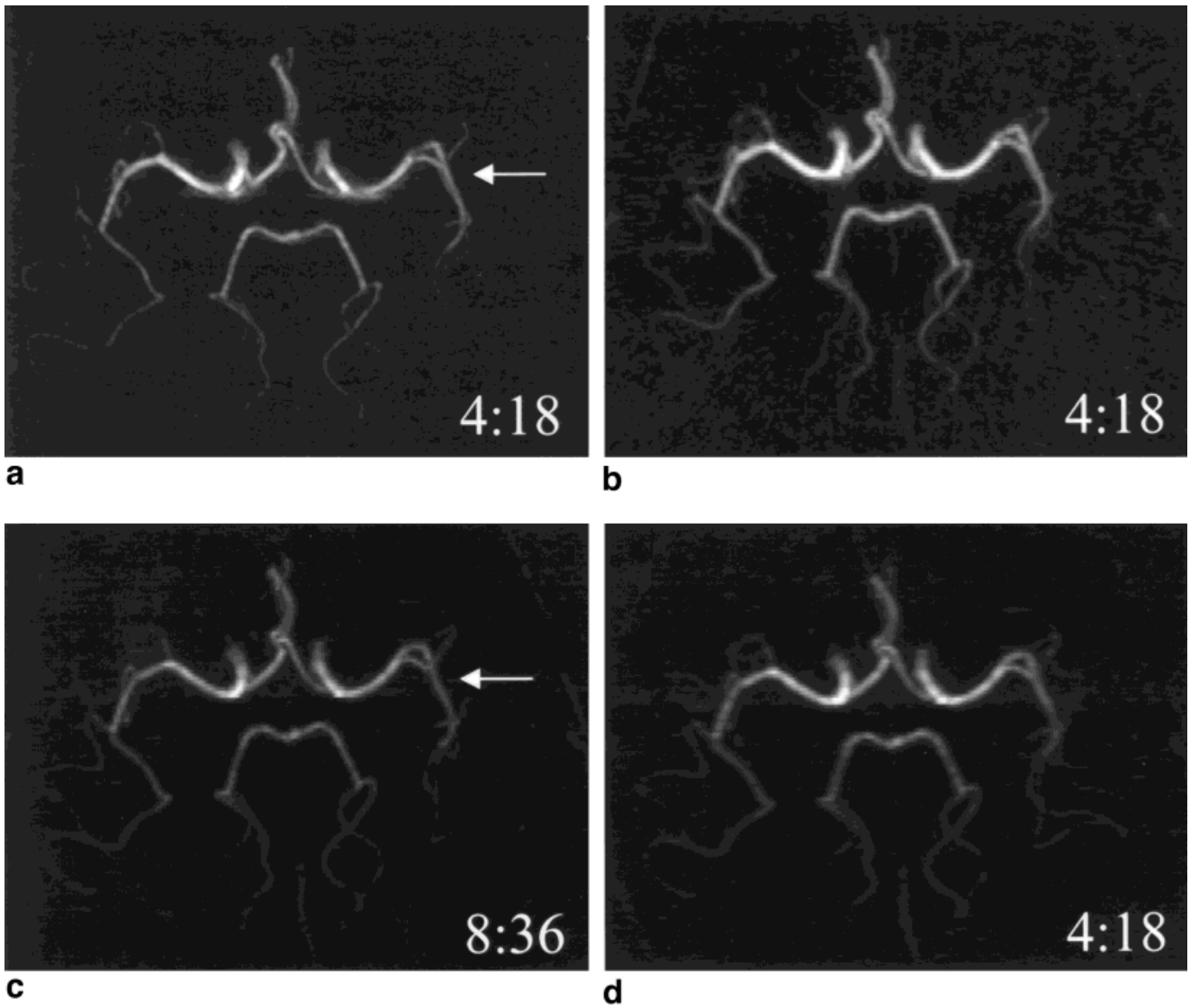

FIG. 6. PIPR (**a,b**) and Cartesian phase-contrast (**c,d**) images of the circle of Willis in a normal volunteer at varying resolutions and scan times. **a:** 512 × 512 PIPR image using 192 projections with a scan time of 4 min 18 sec. **b:** 256 × 256 PIPR image using 192 projections with a scan time of 4 min 18 sec. **c:** 256 × 256 Cartesian PC image with a scan time of 8 min 36 sec. **d:** 256 × 128 Cartesian PC image with a scan time of 4 min 18 sec. The arrows in **a** and **c** point to a region of overlapping vessels where the increased resolution is apparent.

Flow quantification studies were performed for PIPR using a simple tube phantom with constant flow rates ranging between 1.5 ml/sec and 6.0 ml/sec. The calculated flow values vs. the pump setting are shown in Fig. 5.

Human Studies

Figure 6 shows comparisons of axial MIPs obtained with PIPR (top row) and Cartesian trajectory (bottom row) techniques with scan times annotated in the bottom right corner of each image. At the same final image resolution of 256 × 256, the spin-warp scan time of 8 min 36 sec (Fig. 6c) was twice as long as that of PIPR (Fig. 6b). In order to obtain the same scan time of 4 min 18 sec, the Fourier image resolution was decreased to 256 × 128 (Fig. 6d). By doubling the bandwidth and readout resolution (to maintain the same TR), the PIPR resolution could be increased to 410 × 410 (Fig. 6a) without increasing the scan time. A similar doubling of bandwidth and readout resolution could be done with the spin-warp acquisition, but the resolution improvement would only be in the frequency-encoded direction. The SNR of the images was roughly proportional to the voxel size and the square root of the acquisition time for both spin-warp and PIPR.

However, the higher resolution scans often had better than expected SNR, as is possible when the imaged object (in this case, a discrete group of velocities) is smaller than the low-resolution voxel size. The axial MIPs show the increased resolution of PIPR without significant artifacts. The arrows in Fig. 6a,c demonstrate a region where overlapping vessels are better delineated by the high-resolution PIPR scan.

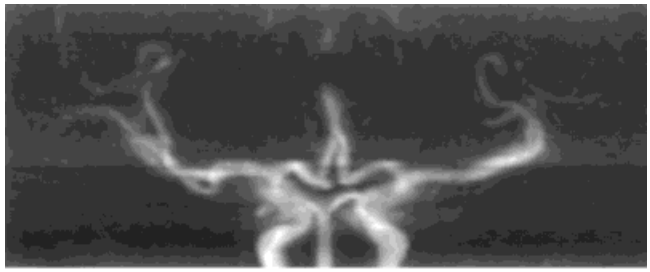

a

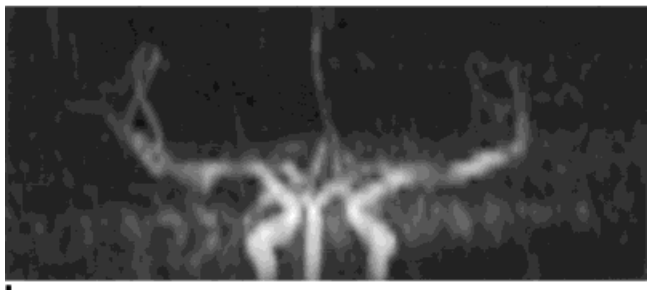

b

FIG. 7. Demonstration of the ability of PIPR to double the number of acquired slices relative to a Cartesian PC acquisition without increasing scan time. The PIPR scan (**a**) was acquired using 180 total projections, 0.9 mm slice thickness, and required a scan time of 8 min 4 sec. Cartesian PC scan (**b**) had 2 mm slice thickness, a full FOV, and required a scan time of 8 min 36 sec. Both images have 256 × 256 in-plane resolution.

Figure 7 is an example of using the time advantage of PIPR to increase resolution in the slice-encoding direction. The PIPR scan (Fig. 7a) was acquired with 64 total slices in a scan time of 8 min 4 sec, whereas the corresponding Fourier scan (Fig. 7b) required 8 min 36 sec to acquire 32 slices. The increased resolution is apparent in the PIPR scan as well as reduced pulsatility artifacts from the carotid arteries.

DISCUSSION

For conventional phase-contrast imaging the spatial resolution in the phase encoding direction is proportional to the number of phase-encoding values acquired. For four-point flow-encoding along all three directions, the scan time is equal to:

$$T_{\text{CARTESIAN}} = N_{PE} \cdot N_Z \cdot TR \cdot 4 \quad [1]$$

where N_{PE} is the number of phase encoding values, N_Z is the number of slices, and the factor of 4 reflects the four-point flow-encoding. As has been previously noted in X-ray CT, the spatial resolution for projection reconstruction techniques is determined by the readout resolution (14). For PIPR the corresponding time for an image with flow-encoding along all three directions is:

$$T_{\text{PIPR}} = N_{\text{PROJ}} \cdot N_Z \cdot TR \cdot 2 \quad [2]$$

where N_{PROJ} is the total number of projections and the factor of 2 in this case reflects the necessary up and down excitations. As the resolution increases, the speed advantage of PIPR also increases. For a 256 × 256 acquisition with 64 slices, and where 192 total projections are used, the time ratio $T_{\text{CARTESIAN}}/T_{\text{PIPR}}$ would be 2.66. In clinical situations the ratio is usually reduced to 2 because a 3/4 rectangular field-of view can be used to decrease the spin-warp acquisition time. For a 512 readout resolution, this ratio becomes 5.22 without partial FOV or 4 when partial FOV is used. At 512 × 512 resolution a phase-contrast scan based on spin-warp techniques becomes impractical because of the very long scan times required.

PIPR acquisitions are limited by SNR at high resolutions. Since the SNR from a six-set acquisition scheme is the same as that from a four-set acquisition scheme (12), the SNR efficiency of PIPR, which utilizes the six-set acquisition scheme to achieve interleaving, is lower than in standard phase-contrast imaging. The high resolution obtainable with PIPR results in smaller voxels and proportionate decreases in SNR. However, if intravoxel dephasing effects are significant, the effect of the small voxel size is mitigated by improved signal from within each voxel. PIPR maintains the same TE as a spin-warp based phase-contrast sequence so there is no difference in flow-dephasing due to TE differences.

At lower resolutions the limiting factor in PIPR acquisitions are the artifacts introduced by undersampling. However, the artifacts seen in PIPR are less severe than those seen in contrast-enhanced angiography and thus the possible time reduction is greater. This is due to two effects. First, the undersampling factor can be made much higher than the factor that can be reliably used with contrast-enhanced angiography. In a phase-contrast image, static tissue and the artifacts that arise from the static tissue subtract out in the final image. In contrast-enhanced angiography, the background signal still contributes artifacts, although these artifacts are at a much lower intensity than the blood signal. Thus even in the individual velocity images the streak artifacts are minimal, provided that greater than approximately 60 projections per velocity direction are acquired. Second, because of the interleaving of velocity directions, the artifacts do not add constructively and their appearance is further reduced in the composite image. Although the interleaving does not reduce the artifacts from objects that are flowing in one predominant velocity direction, it does prevent the artifacts from constructively adding where the flow in a vessel is in multiple directions.

The total number of projections needed also depends on the anatomy and pulsatility of the object to be imaged. The most noticeable streak artifacts emanate from vessels that exhibit the most pulsatility. In the circle of Willis, for example, the internal carotid arteries generate noticeable streak artifact. Thus, cardiac gating might mitigate pulsatility effects and permit even a lower number of projections while still maintaining a low level of artifact.

The pulsatility artifacts that appear as ghosting in standard phase-contrast images appear as streaks in PIPR images. It has previously been noted that the projection reconstruction artifacts for periodically moving objects are quite different from the artifacts of spin-warp imaging (15). Projection reconstruction techniques demonstrate periodic motion as streaks from the varying structure and often appear quite far from the source. In spin-warp based im-

aging the ghosts are all in the phase-encoding direction and have strong intensities close to the source. For nongated scans projection reconstruction methods thus have an intrinsic advantage over spin-warp acquisitions.

CONCLUSIONS

We have shown that an interleaved undersampled projection reconstruction technique can be applied to phase-contrast acquisitions. The technique obtains greater spatial resolution per unit time relative to phase-contrast imaging based on spin-warp techniques. The maximum obtainable resolution with PIPR is limited by the SNR and artifacts rather than scan time. Pulsatility artifacts are reduced in ungated scans. Using projection reconstruction acquisitions for phase-contrast is promising for increasing the feasibility of higher resolution phase-contrast images.

ACKNOWLEDGMENT

A.V.B. is supported by a National Science Foundation Graduate Fellowship.

REFERENCES

1. Hahn EL. Detection of sea water motion by nuclear precession. J Geophys Res 1960;65:776–777.
2. Moran PR. A flow velocity zeugmatographic interlace for NMR imaging in humans. Magn Reson Imaging 1982;1:197–203.
3. Dumoulin CL, Hart HR. Magnetic resonance angiography. Radiology 1986;161:717–720.
4. Nayler GL, Firmin DN, Longmore DB. Blood flow imaging by cine magnetic resonance. J Comput Assist Tomogr 1986;10:715–722.
5. Wigstrom L, Sjoqvist L, Wranne B. Temporally resolved 3D phase-contrast imaging. Magn Reson Med 1996;36:300–803.
6. Wehrli FW, Shimakawa A, Gullberg GT, MacFall JR. Time-of-flight MR flow imaging: selective saturation recovery with gradient refocusing. Radiology 1986;160:781–785.
7. Poncelet BP, Weisskoff RM, Wedeen VJ, Brady TJ, Kantor H. Time of flight quantification of coronary flow with echo-planar MRI. Magn Reson Med 1993;30:447–457.
8. Firmin DN, Gatehouse PD, Longmore DB. Comparison of snap-shot quantitation flow imaging techniques. In: Proceedings of the SMRM, 11th Annual Meeting, Berlin, 1992. p 2915.
9. Pike GB, Meyer CH, Brosnan TJ, Pelc NJ. Magnetic resonance velocity imaging using a fast spiral phase contrast sequence. Magn Reson Med 1994;32:476–483.
10. Peters DC, Korosec FR, Grist TM, Block WF, Vigen KK, Holden JE, Mistretta CA. Undersampled projection reconstruction applied to MR angiography. Magn Reson Med 2000;43:91–101.
11. Bernstein MA, Shimakawa A, Pelc NJ. Minimizing TE in moment-nulled or flow-encoded two- and three-dimensional gradient-echo imaging. J Magn Reson Imaging 1992;2:583–588.
12. Pelc NJ, Bernstein MA, Shimakawa A, Glover GH. Encoding strategies for three-direction phase-contrast MR imaging of flow. J Magn Reson Imaging 1991;1:405–413.
13. Joseph P. Sampling errors in projection reconstruction MRI. Magn Reson Med 1998;40:460–466.
14. Joseph P, Whitley J. Experimental simulation of ECG-gated heart scans with a small number of views. Med Phys 1983;10:444–449.
15. Glover GH, Pauly JM. Projection reconstruction techniques for reduction of motion effects in MRI. Magn Reson Med 1992;28:275–289.